

Proposal of a Geiger-type Single-Phase Liquid Xenon Time Projection Chamber as Future Large Detector for Dark Matter Direct Search

Qing Lin^{a,b,1}

^a*State Key Laboratory of Particle Detection and Electronics, University of Science and Technology of China, Hefei 230026, China*

^b*Department of Modern Physics, University of Science and Technology of China, Hefei 230036, China*

E-mail: qinglin@ustc.edu.cn

ABSTRACT: Dual phase time projection chamber using liquid xenon as target material is one of most successful detectors for dark matter direct search, and has improved the sensitivities of searching for weakly interacting massive particles by almost five orders of magnitudes in past several decades. However, it still remains a great challenge for dual phase liquid xenon time projection chamber to be used as the detector in next-generation dark matter search experiments (about 50 tonne sensitive mass), in terms of reaching sufficiently high field strength for drifting electrons, and sufficiently low background rate. Here we propose a single phase liquid xenon time projection chamber with detector geometry similar to a Geiger counter, as detector technique for future dark matter search. Preliminary field simulation and signal reconstruction study have shown that such single phase time projection chamber is technically feasible and can have sufficiently good signal reconstruction performance for dark matter direct search.

KEYWORDS: Single phase time projection chamber, dark matter detection, liquid xenon detector

¹Corresponding author.

Contents

1	Introduction	1
2	TPCs for Next-Generation Dark Matter Search	2
2.1	Dual Phase Time Projection Chamber	2
2.2	Geiger-type Single Phase Time Projection Chamber	4
3	Drift and Amplification Fields of GS-TPC	5
4	Signal Reconstruction of GS-TPC	8
4.1	Classification of S1 and SE S2	8
4.2	Position Reconstruction	9
5	Summary and Outlook	13

1 Introduction

Dual phase liquid xenon (LXe) Time Projection Chamber (TPC) has been gaining popularity in the field of dark matter direct search during past several decades, thanks to its capability of simultaneously reconstructing scintillation and ionization signals of one event and event vertex. Experiments using such detector technique, like PandaX-I-II [1, 2], XENON100/1T [3, 4], and LUX [5], have been able to keep refreshing the world record of sensitivities for high-mass (>6 GeV) weakly interacting massive particle (WIMP) search. Currently, second-generation dark matter direct search experiments using dual phase LXe-TPC with multi-tonne sensitive mass, such as PandaX-4T [6], XENONnT [7], and LZ [8], are under commissioning and soon will start to collect scientific data, exploring parameter space that is unreachable by previous detectors. However, it remains unclear if dual phase TPC can reach sufficiently good signal quality and ultra-low background level that are required in third-generation dark matter search experiment (~ 50 tonne sensitive mass) [9], to search for dark matter particles that have weaker interaction rate with baryonic matter than current experimental precision. Especially in the sense of reaching high cathode voltage to provide enough drift field strength and of mitigating high isolated ionization background rate, R&D efforts are needed.

On the contrary to the extensive attentions that dual-phase TPCs have received, single phase TPCs have not raised much interest in the field of dark matter direct search. Although single-phase TPC using liquid argon as material has been widely deployed nowadays in large-scale neutrino experiments, such as MicroBooNE [10], ICARUS [11], and DUNE [12], there is no existing dark matter search experiment utilizing such technique. Unlike dual phase TPC which utilize electroluminescence in gas to convert charge signals into proportional lights and collect them, traditional single phase TPC collects charge signals through wire planes [11], thus has a higher

charge collection threshold that is not sufficient for sensitive dark matter direct search. Recent measurements of electroluminescence in LXe [13, 14] have raised new possibilities for single phase LXe TPC that can reach low charge collection threshold. The results in [14] have shown that the proportional lights in LXe start to become visible when the field strength reaches 412 kV/cm. The estimated electron amplification is comparable to the one obtained through electroluminescence in gaseous xenon in a dual phase LXe TPC.

In this manuscript, we propose a single phase LXe TPC which collects charge signals through electroluminescence in LXe and has different geometry than traditional single phase TPC as used in neutrino experiments. In Section 2, a review of dual phase TPC and a description of proposed Geiger-type single phase TPC will be given. In Section 3 and 4, we show the results of field simulation and study of signal reconstruction for such proposed single-phase TPC.

2 TPCs for Next-Generation Dark Matter Search

Dual phase TPC is currently used in second-generation dark matter search experiments, such as PandaX-4T [6], XENONnT [7], and LZ [8], which are under commissioning. It is also the default detector technique that is going to be used in future next-generation dark matter search experiments, like DarkSide-20k [15], DARWIN [9], and PandaX-30T [16]. Although dual phase TPC has shown excellent signal responses (low threshold and high background rejection power) in past experiments, next-generation dual phase TPCs will face non-trivial challenges since they will reach unprecedented size (sensitive mass of about several ten tonne) in the field of dark matter direct search, especially in terms of reaching sufficiently high voltage for drifting electrons and mitigating isolated ionization backgrounds. On the other hand, single phase TPC which collects charge through electroluminescence in LXe is another possible technique that can be used in next-generation detector. The electroluminescence in LXe has been observed and the amplification factor is comparable with the one obtained through electroluminescence in gaseous xenon.

2.1 Dual Phase Time Projection Chamber

Dual phase TPC consists of mainly three parallel plane electrodes, light reflectors and light sensors. PTFEs are traditionally used as light reflectors, and photo-multipliers (PMTs) as light sensors placed at top and bottom of cylindrical TPC sensitive volume. Fig. 1 shows a typical dual phase TPC diagram. Three parallel plane electrodes are (from bottom to top) cathode, gate, and anode. Usually gate electrode is grounded, negative and positive voltages are applied to cathode and anode, respectively. Cathode voltage is typically in the order of several ten kV to provide a drift field strength of several hundred to thousand kV/cm in the sensitive volume. Distance between anode and gate is typically ~ 5 mm, and liquid surface is placed between them. Anode voltage is required to be sufficiently strong so that the field strength in gas is above the threshold for electroluminescence (~ 1.3 kV/cm/atm [17] in gaseous xenon and ~ 0.55 kV/cm/atm [18] in gaseous argon) and gives enough efficiency for extracting electrons out of liquid surface (100% extraction efficiency at ~ 10 kV/cm in gas for xenon [19]). Because of the high voltages applied to cathode and anode and their proximity to the top and bottom PMTs, additional electrode planes (named screen electrodes) are needed in front of top and bottom PMTs for their protection.

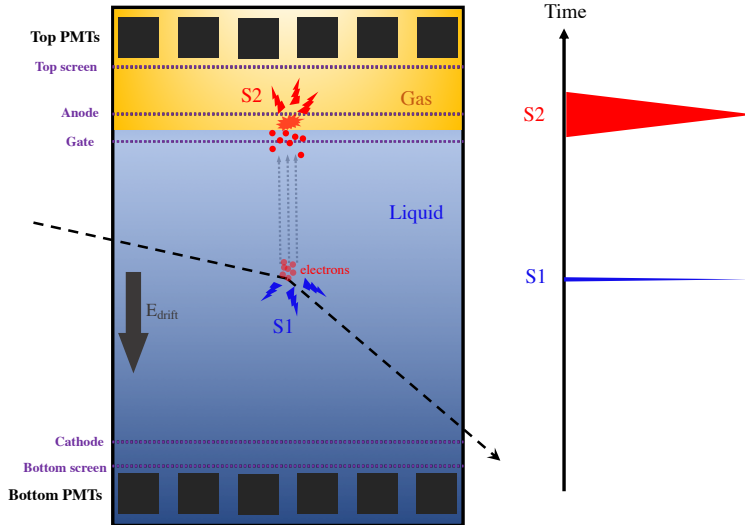


Figure 1: Diagram of a typical dual phase TPC.

The sensitive volume in a dual phase TPC is a cylinder between cathode and gate planes. Deposit energy in sensitive volume is converted into prompt scintillation lights and ionization electrons. Prompt lights are detected by PMTs, and called S1 conventionally. Ionization electrons are drifted towards the proportional amplification region which is between gate and anode planes. Under stronger field in amplification region, electrons are extracted into gas and produce proportional lights which are detected by PMTs and named S2. S1 signal has fast time response in the scale of several ten to hundred nanoseconds, determined by the singlet and triplet decay constant of excimer of target element. On contrary, S2 signal has relatively slow time response in scale of several microseconds, which is dominated by the electron diffusion during drifting and the electron traveling in gas gap after liquid surface extraction. Therefore, S1 and S2 signals are distinguishable on recorded event waveform. The ability to reconstruct the scintillation and ionization signals of an energy deposition is the key of dual phase TPC's success in dark matter direct search. Amplitudes of S1 and S2 signals, as well as the pulse shape information of S1 signal in certain material like argon, can provide discrimination power between electronic recoils (ERs) and nuclear recoils (NRs), and can further reduce the effective backgrounds induced by gamma and betas. In addition, time information of S1 and S2 signals and S2 signal's pattern on PMTs can be used to reconstruct the longitude and transverse positions, respectively, giving 3-D position reconstruction of interaction vertex. This also provides extra rejection power against background from external or material radiations through fiducialization, and against neutron backgrounds through discrimination between single and multiple scatters.

The excellent reconstructions of S1, S2 and event vertex requires high level of field uniformity in both the drift and amplification regions. On the other hand, high transparency of electrode plane is critical in order to maintain a sufficiently high light collection efficiency to search for dark matter signals. This demands the electrode plane to be made of fine wires and maintain good tension on

them under cryogenic temperature, which by itself is a great challenge to multi-ten-tonne dual phase TPC. On top of this, the field strength near cathode wires may be large enough so that the probability of electrons from electrode metal being extracted out through Fowler-Nordheim effect [20] is non-trivial. Extracted electrons can produce proportional scintillation through electroluminescence in liquid material under very strong field near cathode wire, limiting the voltage applied to cathode. Besides, existence of large amount of metal electrodes and liquid surface in dual phase TPC is very likely one of the major causes for large amount of isolated ionization signals (events without a detected over-threshold scintillation signal) in past experiments (such as in XENON100 [19]). Photoionization on metal electrodes produces single- or multi-electron emission, and liquid surface may trap part of the drifted electrons and release them with a time delay [21, 22]. The issues of cathode voltage and isolated ionization signals can become even more critical in next-generation detector as the detector scales up.

2.2 Geiger-type Single Phase Time Projection Chamber

We propose a new single phase TPC with detector geometry similar to a Geiger counter. It amplifies charge signals through electroluminescence in LXe. The simplest conceptual diagram of the proposed Geiger-type single phase TPC can be seen in Fig. 2. Geiger-type Single phase Time Projection Chamber (GS-TPC) has also a cylindrical sensitive volume. Unlike the parallel electrode planes in a dual phase TPC, GS-TPC has parallel wires serving as electrodes. A single wire at the central axis of GS-TPC’s cylinder serves as anode, surrounded by several wires with fixed spacing as gate wires to regulate the amplification fields. Wires at the cylindrical side of GS-TPC’s sensitive volume, parallel to the central axis and equally spaced between adjacent wires, serve as cathode. Light sensors, such as PMTs, can be instrumented to cover the surface of GS-TPC’s cylindrical side.

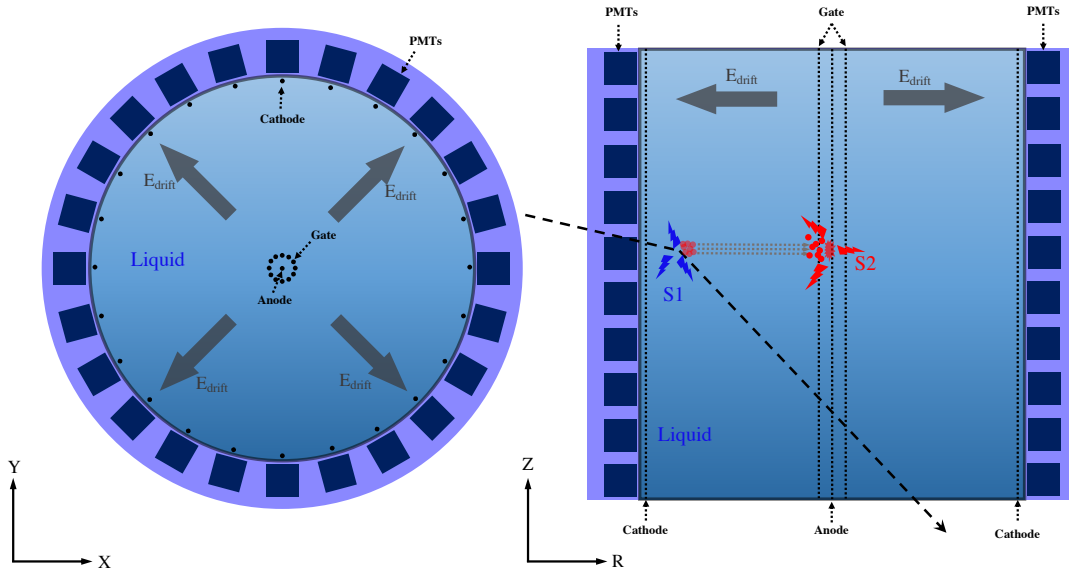


Figure 2: Conceptual diagram of the proposed Geiger-type single phase TPC. Left is the top view, and right plot is the side view.

The signal detection mechanism of GS-TPC is similar to that of a dual phase TPC, but the ionized electrons are drifted to the central axis of sensitive volume, and go through proportional amplification near anode wire. Such a GS-TPC geometry can achieve a field above that is needed for electroluminescence in LXe near anode wire of reasonable macroscopic size, and in the meantime can also maintain moderate field strengths in the active volume between cathode and gate. The most important information is the radial and zenith positions of an event which is required to perform fiducialization of GS-TPC. The radial position in GS-TPC can be reconstructed using the drift time, and the zenith position may be reconstructed using the hit pattern of S2 on light sensors. The angular position is not critical since detector geometry is axial symmetrical. The S2 hit pattern may have “dark zones” because the proportional lights are produced very near anode wire, aiding the reconstruction of angular position to some extent. Compared to the dual phase TPC, the cathode voltage can be much small and still maintain moderate field strength in most part of sensitive volume. The region close to cathode may have low drift field strength and even field distortion, as well as high background rate, and will be removed in analysis. Also, mechanically it is much easier to maintain tension on wires in GS-TPC than wires on electrode planes in dual phase TPC. In addition, absence of liquid surface and less electrode material used can bring less isolated ionization signal in GS-TPC. However, field strength in GS-TPC along radial axis is changing which may bring challenges for reconstructions of energy and radial position. Dedicate calibrations using injected sources, such as ^{83m}Kr [23], with uniform event distribution expected are required to correct the effect brought by non-uniform drift field.

3 Drift and Amplification Fields of GS-TPC

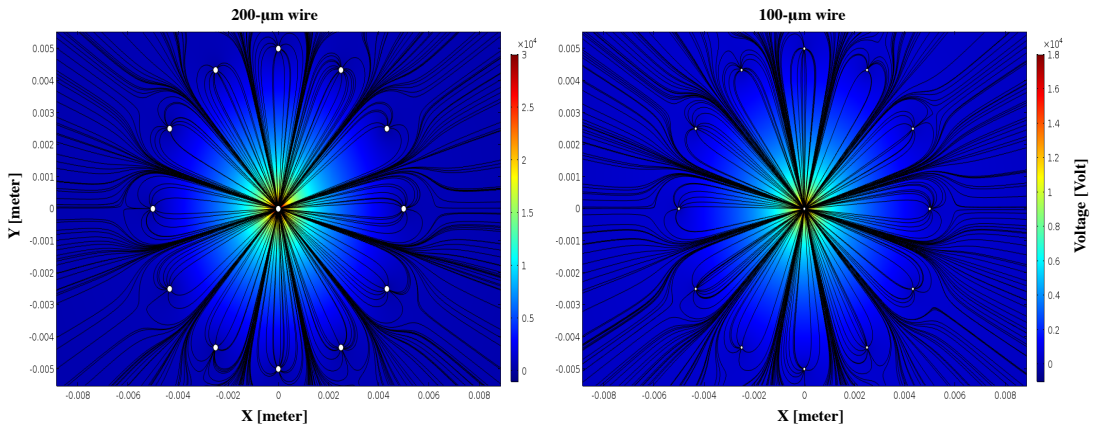


Figure 3: Simulated field lines and voltages in gate-anode region for the prototype GS-TPC. Left plot is for wire with diameter of $200\text{ }\mu\text{m}$ and right plot for wire with diameter of $100\text{ }\mu\text{m}$. The color axes show the voltage at different position.

We have performed field simulations using COMSOL [24], to estimate the field configuration of a prototype GS-TPC and to conduct a feasibility check of such TPC. The prototype GS-TPC is assumed to have a cylindrical sensitive volume with radius of 10 cm, with 36 cathode wires and 12 PMTs instrumented. Twelve gate wires, equally spaced between adjacent wires, are placed 5 mm

away from the central anode wire. Two simulations are performed with different wire diameters, 100 μm and 200 μm , both of which are commercially available wire sizes. Wires made by stainless steel or tungsten with such diameters are anticipated to be strong enough, to tolerate the tension caused by cryogenic shrinking of large-scale GS-TPC. In most commonly used operation mode, cage surface of PMT is set at negative voltage (e.g., about -800 V for R8520 1" Hamamatsu PMT [25]). In order to have minimal amount of electrode wires, there is no screen electrode wires to be placed in front of PMTs in GS-TPC. Therefore, the cathode voltage can not be too high for the protection of the PMTs. In simulations of the prototype GS-TPCs, the cathode voltage is fixed at -1 kV and the gate is grounded.

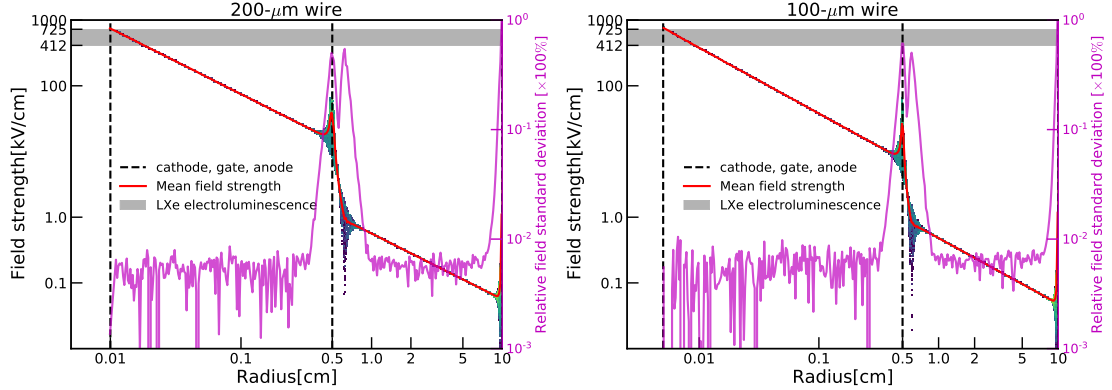


Figure 4: Distribution of TPC volume on field strength vs. radial position. The red and magenta solid lines give the mean and standard deviation of field strength, respectively, at different radial position. The vertical dashed lines indicate the position of gate and cathode wires, respectively. The radius of the prototype GS-TPC is 10 cm. The left and right plots are for prototype GS-TPCs with 200- μm and 100- μm wires, respectively. The shaded regions indicate the allowed field range for electroluminescence in LXe [14]. In the results, gate wires are grounded and cathode wires are set to -1 kV. +30 kV and +18 kV are applied to anode wires for GS-TPCs with 200- μm and 100- μm wires, respectively.

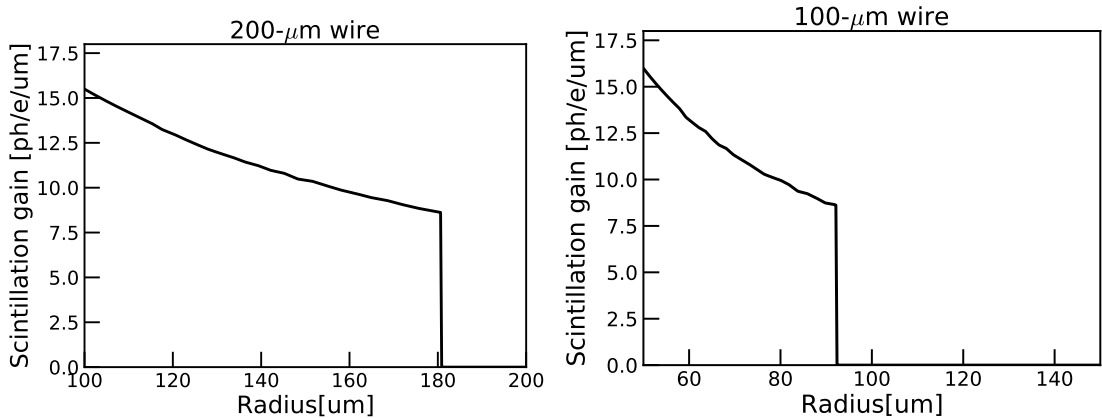


Figure 5: S2 gain as a function of radius for 100- μm (left) and 200- μm (right) anode wires.

Fig. 3 shows the simulated field lines and voltages in gate-anode region for the prototype GS-TPCs with wire diameters of $100\text{ }\mu\text{m}$ and $200\text{ }\mu\text{m}$, respectively. Fig. 4 shows more quantification of field simulation results at different radial positions for aforementioned GS-TPCs. With anode voltage at $+30\text{ kV}$ ($+18\text{ kV}$), prototype GS-TPC with $200\text{-}\mu\text{m}$ ($100\text{-}\mu\text{m}$) wires can surpass the threshold field strength of about 412 kV/cm [14] near anode wire for electroluminescence in LXe. Using the estimated S2 gain factor of $(2.09^{+0.65}_{-0.47})\times 10^{-2}\text{ ph/e}^{-}/(\text{kV/cm})/\mu\text{m}$ obtained by [14], the amplification factors are calculated to be 792^{+246}_{-178} and 409^{+127}_{-92} ph/e^{-} (summarized in Table 1 as well), respectively, for GS-TPC with $200\text{-}\mu\text{m}$ and $100\text{-}\mu\text{m}$ anode wire. The proportional scintillation starts at approximately $80\text{ }\mu\text{m}$ ($41\text{ }\mu\text{m}$) away from the anode wire surface for $200\text{-}\mu\text{m}$ ($100\text{-}\mu\text{m}$) wire, which corresponds to an S2 duration of 31 ns (16 ns) assuming a saturated drift velocity of $\sim 2.578\text{ mm}/\mu\text{s}$ [26]. This indicates that the time profile of the proportional lights in such GS-TPC is dominated by electron diffusion during drift. The relation between proportional scintillation gain and distance to anode wire surface for $100\text{-}\mu\text{m}$ and $200\text{-}\mu\text{m}$ anode wires can be found in Fig. 5.

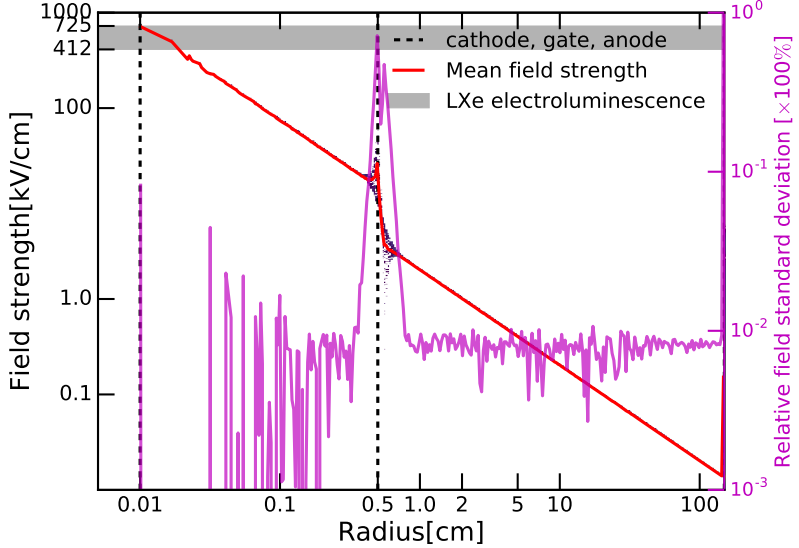


Figure 6: Distribution of TPC volume on field strength vs. radial position for a prototype GS-TPC with radius of 1.5 m . The figure description is the same as in Fig. 4.

Except for the regions that are roughly 1 cm apart from the gate and cathode wires in prototype GS-TPC, the standard deviation of field strength in active volume is at approximately 1% level. In analysis, the regions near gate and cathode are to be removed because of the high expected background rate due to radioactivity in wires and from outside. In active volume with moderate field variance, the field strength ranges from about 80 V/cm near the cathode to about 700 V/cm near the gate. Also the number of gate and cathode wires can be increased in large-scale GS-TPC to provide even lower standard deviation of fields. An additional simulation for large GS-TPC with sensitive volume radius of 1.5 m , 450 cathode wires, $200\text{-}\mu\text{m}$ wires, and 100 PMTs, is performed, which is shown in Fig. 6. The anode and gate voltages are increased to $+40\text{ kV}$ and $+10\text{ kV}$, respectively. Results show that the standard deviation of field strength can reach $\sim 1\%$ in most part of active volume.

Wire diameter [μm]	Anode voltage [kV]	S2 amplification factor [ph/e $^-$]	Singe e $^-$ S2 duration [ns]
100	18	409^{+127}_{-92}	16
200	30	792^{+246}_{-178}	31

Table 1: S2 amplification factors and SE S2 durations for different gate-anode configurations in GS-TPC.

4 Signal Reconstruction of GS-TPC

4.1 Classification of S1 and SE S2

Unlike dual phase TPC which has time duration of about several hundred nanoseconds for S2s caused by single electron (SE), GS-TPC has only couple of tens of nanoseconds for SE signals. Although the large S2 signals still can be distinguished through the signal duration in GS-TPC since electron diffusion dominates the time profile, it has less discrimination power between S1s and SE S2s compared to dual phase TPC. This may cause the increase of isolated S1 signal rate, thus increase of accidental pileup background. We would like to argue that discrimination power can be compensated by classification using pulse shape discrimination (PSD).

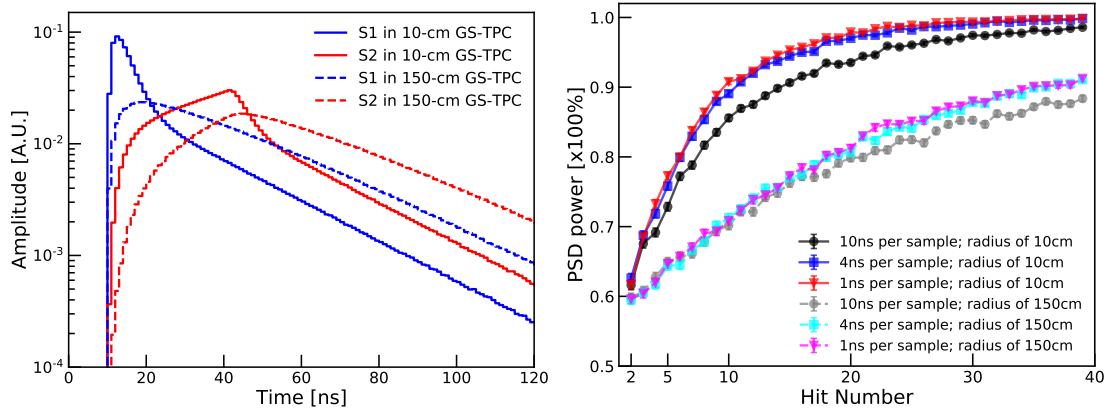


Figure 7: Left plot shows the time profile of S1 and SE S2 in GS-TPCs with radius of 10 cm and 150 cm, respectively. Right plot shows the classification accuracy between S1s and SE S2s, using a simple 2-hidden-layer multi-layer perceptron neural network, as a function of hit number, for GS-TPCs with radius of 10 cm and 150 cm, respectively.

In LXe, the scintillation lights are generated through excimer decay [27] which has two decay components: fast and slow decay components with lifetime of ~ 3 ns and ~ 24 ns [27] corresponding to singlet and triplet state decays, respectively. The ratio between the singlet and triplet components depends on the recoil type [28], and is about 0.8 for ERs and 7.8 for NRs [28]. Therefore, the S1 pulse shape can be modeled as two exponential functions. On the other hand, SE lights are generated, more or less, uniformly along the accelerated electron trajectory near the anode wire (See Fig. 5). Left plot of Fig. 7 shows the expected pulse shape between S1 and SE S2 in GS-TPCs with radius of 10 cm and 150 cm, respectively. The difference in the pulse shapes between 10-cm and

150-cm GS-TPCs is caused by the optical light propagation in detector. The time profile calculation is based on the singlet-to-triplet ratio of 0.8 for ER, which is more conservative in our analysis compared with 7.8 for NR. Also, ERs are the major background in dark matter direct searches. The light propagation in GS-TPC is considered and obtained through optical simulation using GEANT4 toolkit [29]. The pulse shape of single photon hit on light sensors is not taken into account, since the shaping depends greatly on the type of sensor. A classification using multi-layer perceptron (MLP) with 2-hidden-layer is conducted to estimate the PSD power for GS-TPCs with different detector size (radius of 10 cm and 150 cm) and different sampling size (typically 1 ns, 4 ns, and 10 ns per sample). Training and testing samples are sampled using left plot of Fig. 7, giving a uniform hit number distribution between 1 and 40. In the right plot of Fig. 7 shows the PSD power (defined as the accuracy of classification) as a function of hit number. GS-TPC with radius of 150 cm basically has less PSD power over a smaller one with 10-cm radius, because of the smearing of pulse shape due to optical light propagation in detector. PSD power can reach as high as $\sim 97\%$ and $\sim 80\%$ for 10-cm and 150-cm GS-TPCs, respectively, at hit number of 20. However, both PSD powers reduce to about 60% when hit number gets as low as 2. This indicates that reaching high charge amplification factor and high light collection efficiency for proportional scintillation will be important in terms of minimizing the accidental pileup background in such GS-TPC. In addition, the sample size also plays a role in the PSD power for small GS-TPC (improved by approximately 5% when reducing sample size from 10 ns to 4 ns or 1 ns), but makes little difference for large GS-TPC.

4.2 Position Reconstruction

3-D position reconstruction is one of the most critical features of TPC. It allows TPC to be capable of rejecting external gamma-rays and surface backgrounds by fiducialization, discriminating against neutrons by identifying multiple scatters, and reaching high energy resolution by correcting the signals for their spatial dependence. Usually, one spatial coordinate in a TPC is reconstructed through the time difference between scintillation and ionization signals (named drift time) which has relatively high time resolution, and the rest two coordinates are reconstructed using the signal pattern on instrumented sensors (PMTs [30–32] or wire planes in liquid argon TPCs [33, 34]) which is limited by the granularity of sensors. GS-TPC has its radial coordinate reconstructed using drift time, but it does not have very good angular reconstruction resolution because the proportional scintillation occurs in the center axis of the TPC. However as mentioned in previous section, angular distribution of events is less important than radial and zenith distribution for a GS-TPC in dark matter direct search since it provides minor information for rejecting backgrounds and correcting signals in an axial symmetrical detector. The zenith position is, on the other hand, critical for rejecting the backgrounds from two bases of the cylindrical volume (we name the two bases as top and bottom for convenience in later text).

In a prototype GS-TPC as shown in Fig. 2, the hit pattern of the proportional scintillation on PMTs can be used to reconstruct the zenith position. The reconstruction is performed using a Convolutional Neural Network (CNN) based algorithm which is trained on data from optical simulation done using GEANT4 toolkit [29]. Four hundred thousand simulated events are used as training sample, and one hundred thousand are used as testing sample. In simulated events, the number of hits is about 1 k to 2 k. The optical simulation assumes an absorption length of 10 m

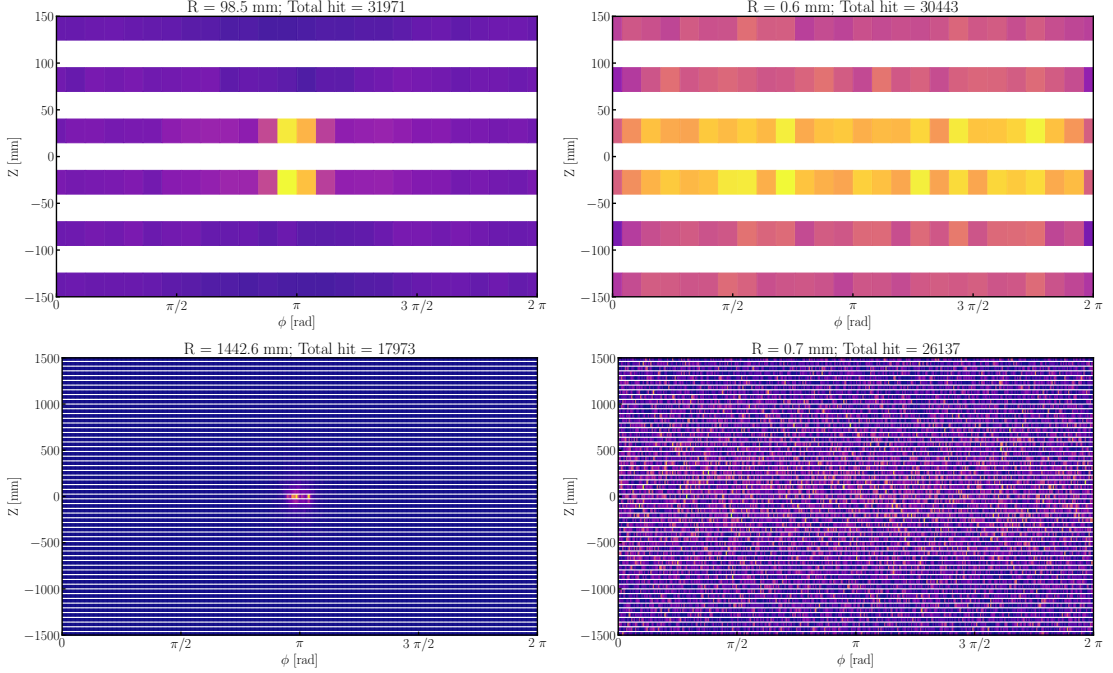


Figure 8: Hit pattern of four sample simulated events. The top and bottom rows are events from GS-TPCs with radius of 10 cm and 150 cm, respectively. The left and right columns are events that are close to side wall and central anode, respectively. The radial position and total hit number of each event are given in the title above each plot.

and Rayleigh scattering length of 50 cm in LXe. The reflectivity of teflon used is assumed to be 99%. Teflon planes are placed at top and bottom of GS-TPCs to increase light collection. The PMT window size is 1-inch square. Two GS-TPCs are simulated: one with radius of 10 cm and height of 30 cm, and the other with radius of 150 cm and height of 300 cm. Numbers of PMT rings are instrumented on the side of GS-TPC. PMT rings are spaced with a fixed distance on Z axis to have a light coverage of 50% on the side wall. There are totally 150 and 21948 PMTs for the GS-TPCs with radius of 10 cm and 150 cm, respectively. The PMT arrangements and hit patterns of four sample signals are shown in Fig. 8. The four sample hit patterns are with events all occur on Y axis and with $Z=0$ mm. Two of them are very close to TPC side, and two of them are near the center axis. Visually, the pattern is more spread as the vertex is further away from the cylindrical side wall, especially for large GS-TPC. Fig. 9 gives the reconstructed Z resolution as a function of Z position of events. For 10-cm radius GS-TPC, the Z resolution can reach approximately 2 cm at the top and bottom, and minimally about 3 mm in the center of TPC. However, the Z resolution of 150-cm radius GS-TPC is much worse because Rayleigh scatter smears out Z information of the original event. The Z resolution is ~ 20 cm at top and bottom, and ~ 4.5 cm in the center.

The Z resolution near top and bottom edges is critical and 20 cm is not an acceptable resolution for future 3rd generation detector. One possible way to improve this is to have light sensors also placed at the top and bottom. Top-bottom asymmetry (TBA) of S2 can provide reconstruction power of Z position. We perform an additional simulation of 150-cm radius GS-TPC with 41×41 PMTs

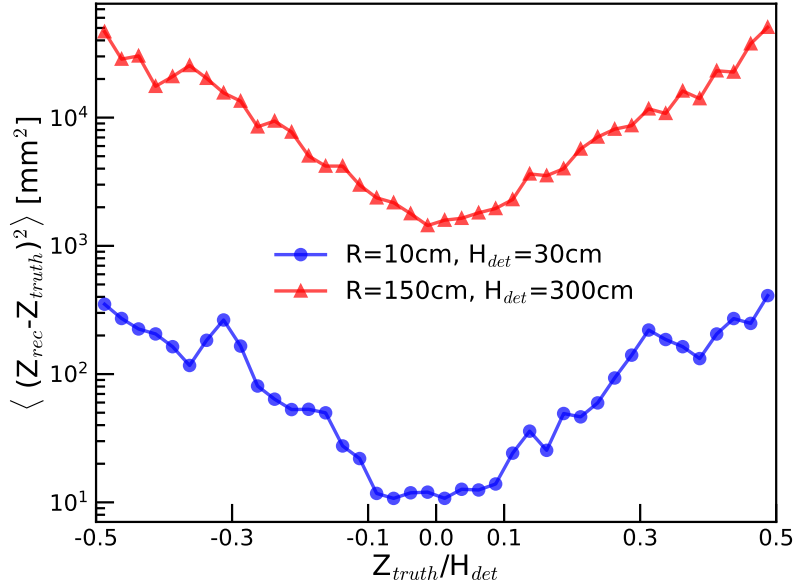


Figure 9: PMT pattern reconstructed Z resolution as a function of Z normalized by detector height. The blue circles and red triangles represent the results from GS-TPCs with radius of 10 cm and 150 cm, respectively.

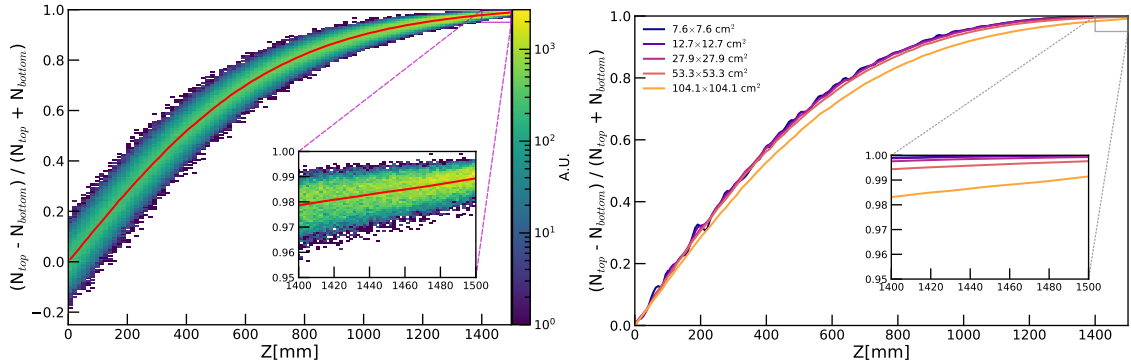


Figure 10: Left plot shows TBA distribution of simulated events in a GS-TPC with radius of 150 cm and height of 300 cm. 1681 PMTs (41×41) are placed at both top and bottom. Right plot shows the expected TBA as a function of Z for different scenarios of number of kept top/bottom PMTs.

matrix at both top and bottom surfaces. Each matrix covers roughly a 1 m×1 m area. The Z positions of simulated events are sampled uniformly from -150 cm to 150 cm (with 0 as the center of GS-TPC). In Fig. 10, the left plot shows the TBA distribution of 1 million simulated events and mean TBA as a function of Z position, which can be used to reconstructed Z . It is worth noting that placing light sensors at top and bottom of GS-TPC may bring challenges in maintaining good field uniformity in top and bottom regions, and may increase radioactive background (gamma-rays and neutrons) from PMT material. It is preferable to minimize the number of PMTs at top and bottom. In this work, we check the reconstruction results with different number of 1-inch PMTs placed in the central area of the top and bottom basis plane: 3×3, 5×5, 11×11, 21×21, and 41×41 PMTs, corresponding to

area coverage of 7.6×7.6 , 12.7×12.7 , 27.9×27.9 , 53.3×53.3 , and $104.1 \times 104.1 \text{ cm}^2$. Right plot of Fig. 10 gives the expected TBA (with sufficiently large number of hits on top and bottom PMTs) as a function of Z position, for different scenarios of number of top/bottom PMTs as mentioned above. Using simple toy MC, we can derive the resolution of TBA-based position reconstruction. Fig. 11 shows the bias and resolution of TBA-based reconstruction as a function of Z with number of hits on top/bottom PMTs of 10, 100 and 1000, respectively. The reconstruction resolution $\sqrt{D(Z_{rec})}$ is defined as the standard deviation of reconstructed Z . The left column of Fig. 11 shows that the TBA-based reconstruction has large bias due to very low statistics of number of hits, as well as $>10 \text{ cm}$ resolution. Most importantly due to the low light collection efficiency of the opposite PMTs, the TBAs of events near top/bottom basis surface are most likely to be 1, leading to large bias and reduced reconstruction power near top/bottom surface, the region of which is of the most interest in terms of background rejection through fiducialization. Despite the regions near top and bottom edges, the reconstruction performances between different scenarios of number of kept PMTs have minor difference.

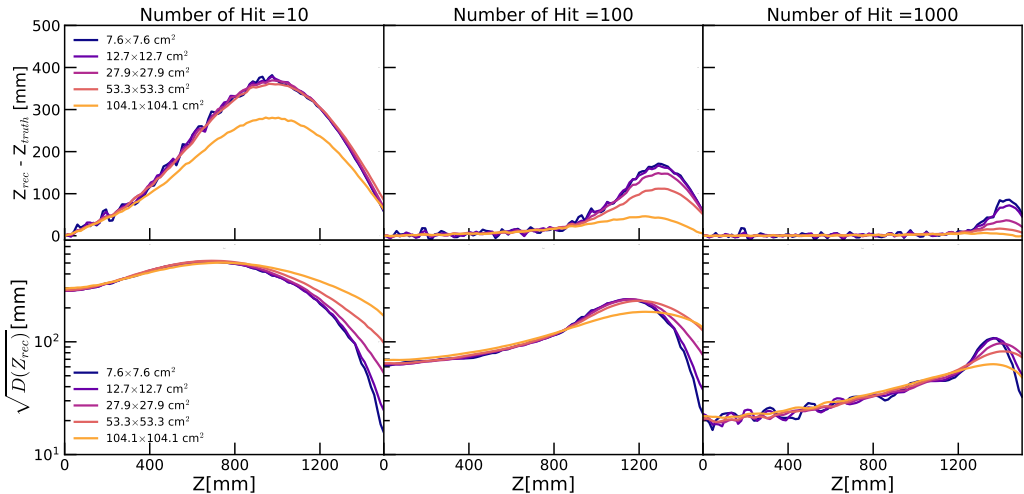


Figure 11: Top and bottom rows show the bias and resolution of TBA-based reconstruction, respectively, for different scenarios of number of kept PMTs. The left, middle, and right columns give the bias and resolution with number of hits of 10, 100, and 1000, respectively.

Besides TBA, the hit pattern on top/bottom PMTs can be used to conduct Z reconstruction, especially in near top/bottom regions because of the proximity of top/bottom PMTs to proportional lights. Fig. 12 shows the normalized hit pattern on top PMTs (41x41) of four sample events with different distances to top plane. Number of hits for these events and later samples in CNN reconstruction are roughly between 700 to 3000, depending on number of kept PMTs. It is visible that the hit pattern gets more spread as the event happens closer to top. We perform CNN-based reconstruction for different scenarios of kept number of PMTs. There is minor difference in the performance of the reconstruction for different scenarios. The slight difference between different scenarios can be due to the different CNN architecture (depth and complexity), which is out of scope of this work and can be further optimised with realistic detector. The results are shown in Fig. 13. In the region that is within 10 cm away from top/bottom plane, the resolution of Z that

is reconstructed using hit pattern on top/bottom PMTs can reach sub-cm level when hit number is at about one thousand. In addition, it does not need a large number of PMTs covering top/bottom plane to reach a high Z resolution. Fig. 13 shows that the nine PMTs in the very center of top/bottom plane have the most pattern information for reconstruction.

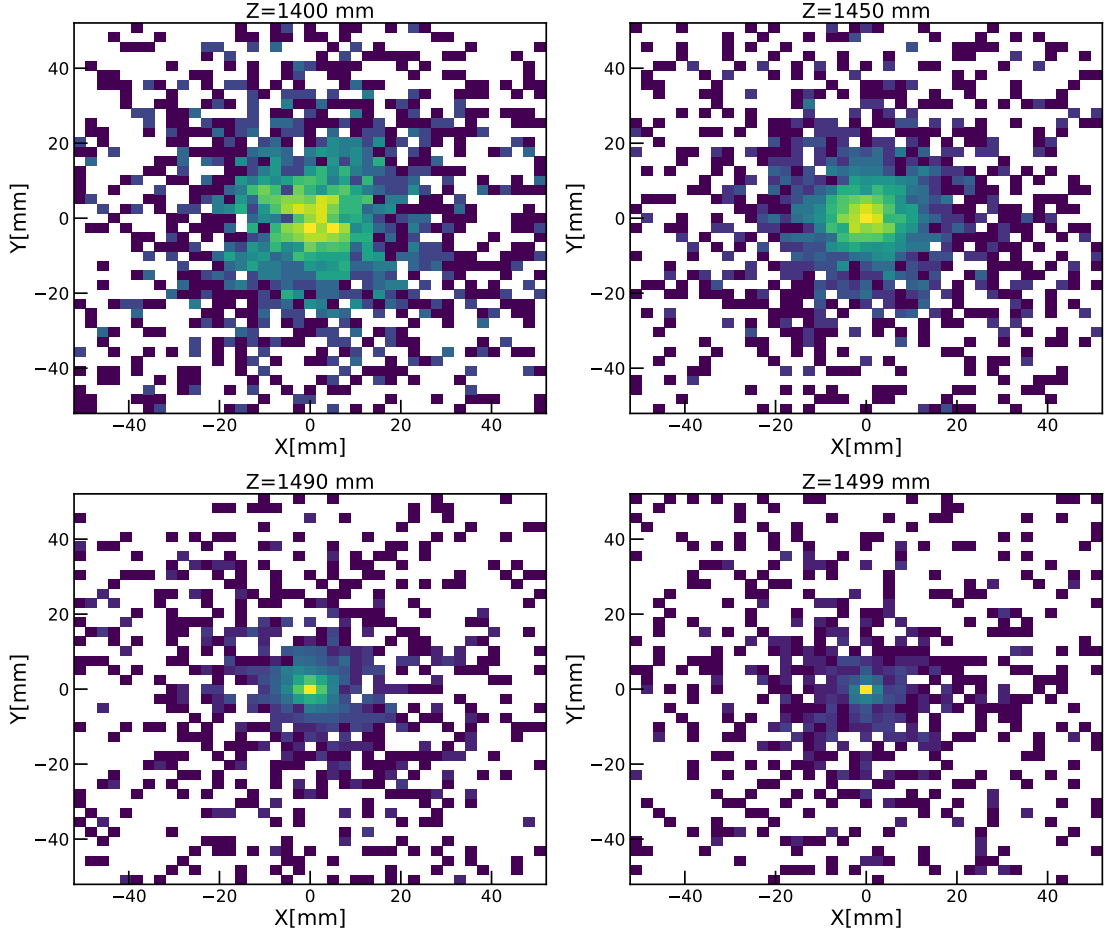


Figure 12: Hit patterns on top 41×41 PMTs of simulated events. Four events happen 100, 50, 10, and 1 mm away from top plane, respectively.

5 Summary and Outlook

We propose a new type of single phase TPC (GS-TPC), which has detector geometry similar to a Geiger counter and has the potential to be used as dark matter direct search detector in future experiment. With a single wire as anode at central axis of cylindrical sensitive volume, the field strength near the anode wire can reach the threshold field strength for electroluminescence in LXe (420 kV/cm) with moderate voltages applied. Such GS-TPC conceptually can reduce the rate of isolated small ionization signals which can affect the signal reconstruction and form accidental backgrounds, reducing dark matter search sensitivity. GS-TPC has no liquid-gas surface so that it has no small ionization signals coming from delayed extraction of electrons [21, 22]. Besides, GS-

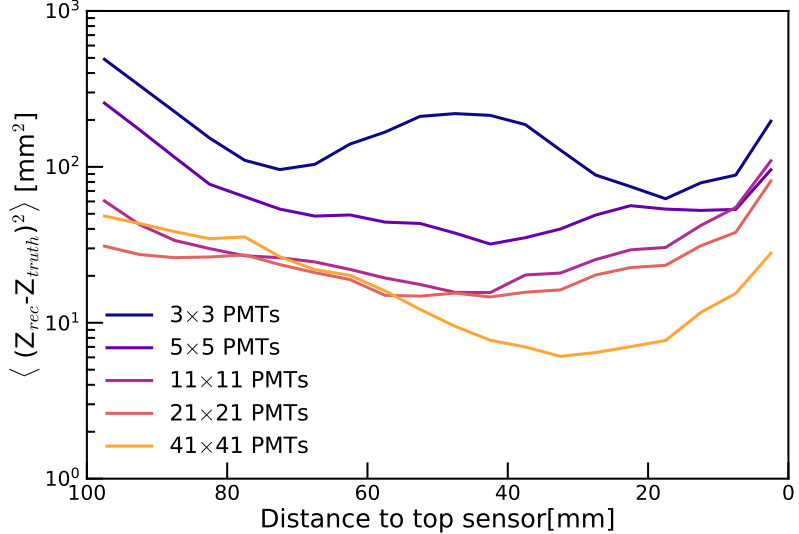


Figure 13: Reconstruction resolution as a function of distance to top plane for different scenarios of kept number of PMTs.

TPC can have minimal field strength around cathode wires, mitigating the electron emission from metal wire through Fowler-Nordheim effect [20]. In addition, GS-TPC has less mechanic demands on electrode compared to a dual-phase TPC which can help to maintain the stable operation in large detector.

On the other hand, the challenges are that GS-TPC has non-uniform field in sensitive volume along radial position, proportional lights for a single electron has time profile close to prompt scintillation lights, and position reconstruction. Field simulation shows that in most part of GS-TPC's active volume, the standard deviation of field strength can reach approximately 1% level. It is able to reach good signal quality with correction for GS-TPC's radial dependence of field. The time duration of SE S2s in GS-TPC is similar to that of prompt S1, but do have different pulse shape. We have performed simple MLP-based classification between S1s and SE S2s in GS-TPC using toy MC data. Results show that PSD classification power can reach about 90% when the light collection of S2 is sufficiently large to have SE S2 at >40 hits. The digitizer sampling rate plays a minor role in the classification performance. Radial positions of events in GS-TPC are reconstructed using drift time, thus having high resolution. Angular positions are with low resolution due to Rayleigh scattering and finite number of gate wires in large GS-TPC. However angular information of events is not critical in an axial symmetrical detector. Z positions of events in GS-TPC are of great importance in terms of rejecting external gamma-rays and surface backgrounds. Using hit pattern on detector side, the Z reconstruction quality is not good (~ 20 cm near top/bottom) due to the fact that PMTs are far away from detector central axis where S2s are produced. Instrumenting light sensors on top and bottom surfaces can greatly improve the resolution of Z position reconstruction in GS-TPC, both through the top-bottom asymmetry and reconstruction using hit pattern. In regions near top/bottom planes, the best Z resolution estimated can reach sub-cm level for hit number of ~ 1000 hits.

In summary, GS-TPC is conceptually a promising technique that can be used in future dark

matter direct search experiment with low isolated S2 signals and low accidental pileup backgrounds. However, realistic mechanical precision may affect GS-TPC's performance which needs R&D work to demonstrate. For example, the surface smoothness of anode wire may violate the axial symmetry of GS-TPC, which needs extra treatment. Also, it is challenge to place PMTs at top/bottom planes in GS-TPC. Shielding electrodes are needed to protect PMTs and to avoid field distortion in top/bottom regions. Other light sensors, such as SiPMT, and special light collection techniques, such light guides coupled with PMTs, need to be explored.

References

- [1] X. Xiao et al. (PandaX-I), *Phys. Rev. D* **92**, 052004 (2015).
- [2] A. Tan et al. (PandaX-II), *Phys. Rev. Lett.* **117**, 121303 (2016).
- [3] E. Aprile et al. (XENON100), *Phys. Rev. Lett.* **109**, 181301 (2012).
- [4] E. Aprile et al. (XENON1T), *Phys. Rev. Lett.* **121**, 111302 (2018).
- [5] D. Akerib et al. (LUX), *Phys. Rev. Lett.* **118**, 021303 (2017).
- [6] H. Zhang et al. (PandaX-4T), *Science China Physics, Mechanics & Astronomy* **62**, 31011 (2019).
- [7] E. Aprile et al. (XENONnT), *Journal of Cosmology and Astroparticle Physics* **2020**, 031 (2020).
- [8] D. Akerib, C. Akerlof, S. Alsum, H. Araújo, M. Arthurs, X. Bai, A. Bailey, J. Balajthy, S. Balashov, D. Bauer, et al., *Physical Review D* **101**, 052002 (2020).
- [9] J. Aalbers et al., *Journal of Cosmology and Astroparticle Physics* **2016**, 017 (2016).
- [10] R. o. Acciarri (MicroBooNE), *Journal of Instrumentation* **12**, P02017 (2017).
- [11] R. Acciarri, C. Adams, R. An, C. Andreopoulos, A. Ankowski, M. Antonello, J. Asaadi, W. Badgett, L. Bagby, B. Baibussinov, et al., *arXiv preprint arXiv:1503.01520* (2015).
- [12] B. Abi, R. Acciarri, M. Acero, M. Adamowski, C. Adams, D. Adams, P. Adamson, M. Adinolfi, Z. Ahmad, C. Albright, et al., *arXiv preprint arXiv:1807.10334* (2018).
- [13] L. Arazi, A. Coimbra, R. Itay, H. Landsman, L. Levinson, B. Pasmantirer, M. Rappaport, D. Vartsky, and A. Breskin, *Journal of Instrumentation* **8**, C12004 (2013).
- [14] E. Aprile, H. Contreras, L. Goetzke, A. M. Fernandez, M. Messina, J. Naganoma, G. Plante, A. Rizzo, P. Shagin, and R. Wall, *Journal of Instrumentation* **9**, P11012 (2014).
- [15] C. E. Aalseth, F. Acerbi, P. Agnes, I. Albuquerque, T. Alexander, A. Alici, A. Alton, P. Antonioli, S. Arcelli, R. Ardito, et al., *The European Physical Journal Plus* **133**, 131 (2018).
- [16] J. Liu, X. Chen, and X. Ji, *Nature Physics* **13**, 212 (2017).
- [17] E. Aprile, K. L. Giboni, P. Majewski, K. Ni, and M. Yamashita, *IEEE Transactions on nuclear science* **51**, 1986 (2004).
- [18] C. M. B. Monteiro, *Ph.D. thesis* (2011).
- [19] E. Aprile et al. (XENON100), *Journal of Physics G: Nuclear and Particle Physics* **41**, 035201 (2014).
- [20] E. Bodnia, E. Bernard, A. Biekert, E. Boulton, S. Cahn, N. Destefano, B. Edwards, M. Gai, M. Horn, N. Larsen, et al., *arXiv preprint arXiv:2101.03686* (2021).
- [21] P. Sorensen, *arXiv preprint arXiv:1702.04805* (2017).

- [22] P. Sorensen and K. Kamdin, arXiv preprint arXiv:1711.07025 (2017).
- [23] L. Kastens, S. Cahn, A. Manzur, and D. McKinsey, *Physical Review C* **80**, 045809 (2009).
- [24] C. Multiphysics, COMSOL Multiphysics, Burlington, MA, accessed Feb **9**, 2018 (1998).
- [25] E. Aprile, M. Beck, K. Bokeloh, R. Budnik, B. Choi, H. Contreras, K.-L. Giboni, L. Goetzke, R. Lang, K. Lim, et al., *Journal of Instrumentation* **7**, P10005 (2012).
- [26] E. Aprile and T. Doke, *Reviews of Modern Physics* **82**, 2053 (2010).
- [27] V. Chepel and H. Araújo, *Journal of Instrumentation* **8**, R04001 (2013).
- [28] J. Mock, N. Barry, K. Kazkaz, D. Stolp, M. Szydagis, M. Tripathi, S. Uvarov, M. Woods, and N. Walsh, *Journal of Instrumentation* **9**, T04002 (2014).
- [29] S. Agostinelli, J. Allison, K. a. Amako, J. Apostolakis, H. Araujo, P. Arce, M. Asai, D. Axen, S. Banerjee, G. . Barrand, et al., *Nuclear instruments and methods in physics research section A: Accelerators, Spectrometers, Detectors and Associated Equipment* **506**, 250 (2003).
- [30] E. Aprile, J. Aalbers, F. Agostini, M. Alfonsi, F. Amaro, M. Anthony, B. Antunes, F. Arneodo, M. Balata, P. Barrow, et al., *The European Physical Journal C* **77**, 1 (2017).
- [31] X. Cao, X. Chen, Y. Chen, X. Cui, D. Fang, C. Fu, K. L. Giboni, H. Gong, G. Guo, M. He, et al., *Science China Physics, Mechanics & Astronomy* **57**, 1476 (2014).
- [32] D. Akerib, C. Akerlof, D. Y. Akimov, S. Alsum, H. Araújo, X. Bai, A. Bailey, J. Balajthy, S. Balashov, M. Barry, et al., arXiv preprint arXiv:1509.02910 (2015).
- [33] S. Amerio, S. Amoruso, M. Antonello, P. Aprili, M. Armenante, F. Arneodo, A. Badertscher, B. Baiboussinov, M. B. Ceolin, G. Battistoni, et al., *Nuclear Instruments and Methods in Physics Research Section A: Accelerators, Spectrometers, Detectors and Associated Equipment* **527**, 329 (2004).
- [34] M. Soderberg and M. Collaboration, in *AIP Conference Proceedings* (American Institute of Physics, 2009), vol. 1189, pp. 83–87.